The fluid–solid equilibrium for a charged hard sphere model revisited

Carlos Vega, José L. F. Abascal, and Carl McBride
Departamento de Química-Física, Facultad de Ciencias Químicas, Universidad Complutense de Madrid, E-28040 Madrid, Spain

Fernando Bresme[a)]
Department of Chemistry, Imperial College of Science, Technology and Medicine, Exhibition Road, London SW7 2AY, United Kingdom

(Received 5 March 2003; accepted 31 March 2003)

The global phase diagram of a system of charged hard spheres, composed of positive and negative ions of the same size, is obtained by means of computer simulations. Thermodynamic integration and Einstein crystal calculations are used to determine the free energies of the different possible solid structures. In this way, the fluid–solid and solid–solid phase transitions are located. Gibbs–Duhem integration is used to trace the full coexistence curves between the different phases involved. Three different solid structures are found to be stable for the model considered; namely, a cesium chloride structure (CsCl), a substitutionally disordered close packed structure which is faced centered cubic (fcc), and a tetragonal ordered structure with a fcc arrangement of atoms if the charge of the ions is not considered. At high temperatures, freezing leads to the substitutionally disordered close packed structure. This solid structure undergoes an order–disorder transition at low temperatures transforming into the tetragonal solid. At low temperatures freezing leads to the cesium chloride structure (CsCl) which undergoes a phase transition to the tetragonal structure at high pressures. The tetragonal solid is the stable solid phase at low temperatures and high densities. In a narrow range of temperatures direct coexistence between the fluid and the tetragonal solid is observed. Three triple points are found for the model considered. The usual vapor–liquid–CsCl solid triple point occurs at $T^*=0.0225$. In addition, a fluid-fcc disordered-tetragonal triple point is located at $T^*=0.245$ and, finally, a fluid-CsCl-tetragonal triple point appears at $T^*=0.234$. The results presented here can be used to test the performance of the different theoretical treatments of freezing available in the literature. © *2003 American Institute of Physics.*
[DOI: 10.1063/1.1576374]

I. INTRODUCTION

The structure of molecular fluids at high densities is dominated by repulsive forces.[1,2] Hence, the study of models having only repulsive interactions, for instance hard bodies, is of great importance. In the case of ionic systems the structure is determined simultaneously by short range repulsive forces and by long range coulombic interactions. For this reason, the study of a hard ionic system may be of great value in improving our understanding of ionic systems in general. This paper is devoted to one of the simplest hard ionic models; a charged hard sphere system usually known as the restricted primitive model (RPM). The RPM has played a fundamental role in the study of ionic systems, in some sense analogous to the role played by the hard sphere model in the study of neutral systems. It consists of a mixture of hard spheres, one-half being positively charged and the other half being negatively charged. The absolute value of the charges, as well as the particle diameters, are the same for both species.

A particularly interesting problem is the determination of the global phase diagram of the RPM. The existence of a vapor–liquid phase transition in this model was shown by Vorontsov-Vel'yaminov and Chasovskikh by means of Monte Carlo computer simulations.[3,4] Stell *et al.*,[5] by means of theory, also predicted the existence of a vapor–liquid equilibrium. Recent computer simulations[6–11] have now established definitively the existence of the vapor–liquid equilibrium for the restricted primitive model and the location of the critical point. Also, very recently results of the liquid–vapor surface tension of the RPM have been published[12,13] which show excellent agreement with experimental results for ionic salts. The nature of the critical point of ionic fluids has also been the focus of a number of studies.[14–18] The study of the fluid–solid equilibrium of the model has, however, received comparatively less attention. In 1968, Stillinger and Lovett[19] outlined the first approximation of the RPM phase diagram, including the fluid–solid transition. Twenty years later, Barrat[20] used density functional theory (DFT) in the description of the freezing of the RPM model. Simulation results for the fluid–solid equilibrium of the model were presented in 1996 by Smit *et al.*[21] and by Vega *et al.*[22] Each of the aforementioned studies showed that, at low temperatures, the stable structure of the solid is the same as that of solid cesium chloride. At high temperatures the stable RPM solid exhibits a face centered cubic (fcc) structure with a random allocation of cations and anions. The situation seemed clear until Bresme *et al.*[23] found that, at low

[a)]Also at Departamento de Química-Física, UCM.

temperatures, the ions of the substitutionally disordered fcc structure spontaneously undergo an order–disorder transition. Therefore, besides the CsCl and disordered fcc structures, another type of solid, stable at low temperatures and high densities, is present in the RPM phase diagram. In this new phase the ions also form a fcc lattice; however, rather than being randomly allocated they have long range substitutional order. Despite the positional fcc symmetry, the symmetry of the system unit cell (see Ref. 23) is tetragonal when substitutional order is considered. Theoretical attempts to describe this type of order–disorder transition (although for different lattice structures) have been recently proposed.[18,23,24]

In a previous communication by ourselves[23] a preliminary phase diagram of the RPM was presented. In this work a number of issues raised in Ref. 23 are expanded upon, and new calculation results are presented. For instance, results were presented in graphical form. In this paper the simulation results are provided in a tabular format to aid comparison with theoretical results for the fluid–solid equilibrium of ionic systems. As well as this a number of additional coexistence points for the fluid–solid coexistence curve have been calculated, leading to a smoother phase diagram. However, the primary motivation for the present work is to present the results of various calculations that complement and expand upon the results of Ref. 23. In our previous work, the order-disorder phase transition was obtained via NVT simulations (at constant density) using a cubic unit cell. It has been mentioned that the ordered fcc phase has tetragonal symmetry. Therefore, the order–disorder transition, which is likely to be first order (see Ref. 25), can only be located precisely when the tetragonal symmetry of the ordered solid phase is considered in the calculations. One possible route to correctly treating the tetragonal phase is to use an anisotropic NpT first proposed by Rahman and Parrinello[26] and later extended to Monte Carlo simulations by Yashonath and Rao.[27] Another aspect of the previous work, which is improved upon here, is the way in which the free energy of the ordered phase is evaluated. In Ref. 23 thermodynamic integration was used to obtain the free energy of the ordered solid phase from the free energy of the fcc disordered solid. Although the thermodynamic cycle showed that this procedure was consistent, rigorously speaking one cannot use thermodynamic integration when crossing a first order phase transition (notice however that the density jump between the ordered and disordered solid is very small indicating that the transition is only weakly first order). In order to check the validity of the thermodynamic integration approximation, an alternative method of computing the free energy of the ordered solid would be of interest. For that purpose, the free energy of the substitutionally ordered solid can be calculated using the Einstein crystal methodology.[28–30]

In summary, this work intends to provide a detailed view of the phase diagram of the RPM model, rigorously treating the ordered solid phase by using anisotropic NpT simulations and determining its free energy using Einstein crystal calculations. To obtain smooth fluid–solid and solid–solid coexistence curves we use the Gibbs–Duhem integration method as proposed by Kofke.[31,32] The scheme of this paper is as follows: In Sec. II we report the details of the computer simulations performed in this work. In Sec. III the results of this work will be presented, and, in Sec. IV, the conclusions will be summarized.

II. SIMULATION DETAILS

The restricted primitive model is defined as an equimolar-equisized mixture of anions and cations which interact via the potential

$$u(r)=u_{\mathrm{HS}}+u_{qq}=u_{\mathrm{HS}}\pm q^2/(\epsilon r), \tag{1}$$

where u_{HS} is the hard sphere potential, q is the ionic charge, ϵ is the dielectric constant of the medium, and σ the hard sphere diameter. In Eq. (1) the plus and minus signs apply to interactions between ions of the same or opposite charge sign, respectively. The reduced number density of the system is defined in terms of σ as, $\rho^*=\rho\sigma^3=(N/V)\sigma^3$, with N being the total number of ions filling a volume V and ρ the number density. Similarly, the reduced temperature is defined as $T^*=1/\beta^*=kT\epsilon\sigma/q^2$, with k being the Boltzmann constant and T the temperature. Finally, the reduced pressure is $p^*=p\epsilon\sigma^4/q^2$.

When working with charged systems, one is forced to carefully consider the computation of the Coulombic contribution to the potential energy. In this work, the Ewald summation method[33,34] is employed. In the Ewald method, the coulombic potential is divided into two contributions, one is computed in the real space whilst the other being calculated in reciprocal space. The relative importance of these contributions is controlled by a parameter α. In this work $\alpha=0.863/\sigma$. Interactions in real space were truncated at 2.9σ. The reciprocal space is restricted to the vectors $\mathbf{h}$ such that the modulus of the vector is $|\mathbf{h}|^2<27$. In addition, the system considered is surrounded by a conductor. It has been checked that this set of parameters is able to correctly reproduce the Madelung constant of the two lattices (CsCl and tetragonal) involved in this work.

For completeness, the unit cells of the solid phases are displayed in Fig. 1. In Fig. 1(a), the well known cesium chloride structure is presented. Figure 1(b) shows a disordered fcc unit cell and Fig. 1(c) depicts the low temperature tetragonal solid structure. These structures will be denoted more succinctly as CsCl, fcc disordered, and tetragonal structure, respectively. Notice that the tetragonal structure can be obtained from the replication of two fcc unit cells along the c direction. At close packing $[\rho^*=\sqrt{(2)}]$, each ion has 12 ions at a distance $r=\sigma$; out of these 12 nearest neighbors, 8 have a charge with opposite sign to that of the central ion, and 4 have the same charge sign. In these conditions, the c axis length is simply double that of the a and b axes (the c axis, as usual, is taken to be along the direction that breaks the cubic symmetry of the cell). At densities below that of close packing, the tetragonal symmetry of the system is reflected in the axes lengths, i.e., $a=b$ but $c/(2a)\neq 1$. This is because, for densities smaller than that of close packing, the ions with opposite charge sign tend to be closer to a given ion than those with the same charge sign. Given this one

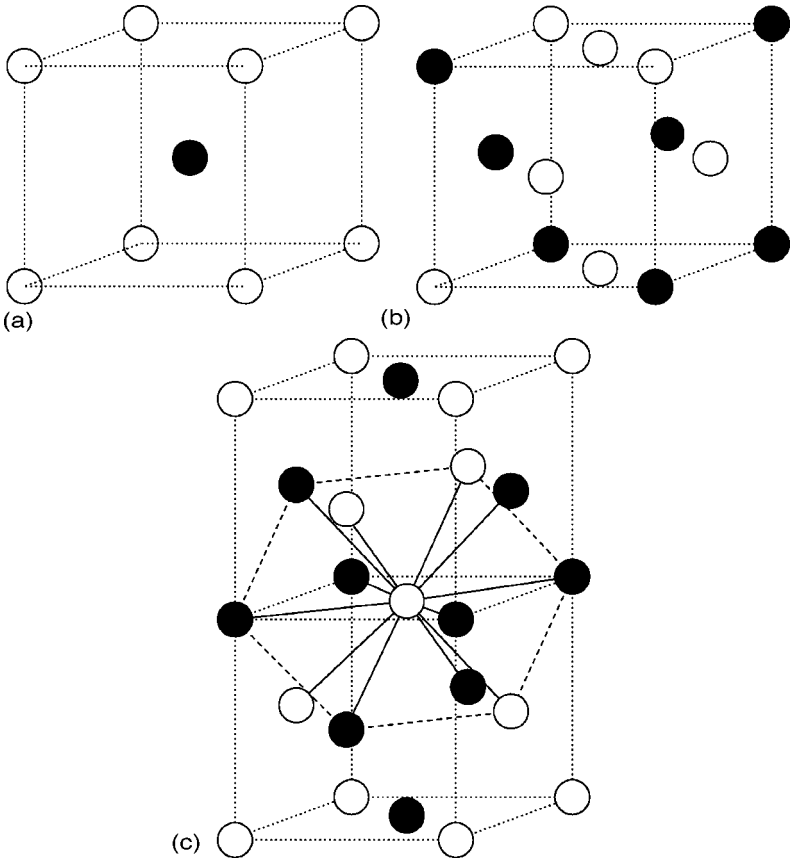

FIG. 1. Solid structures considered in this work. (a) CsCl like unit cell; (b) disordered fcc structure (made of substitutionally disordered ions on a fcc structure); (c) a tetragonal unit cell which correspond to a substitutionally ordered fcc lattice. The space group of the unit cell is tetragonal $I\bar{4}m2$.

expects the ratio $c/(2a)\geqslant 1$. The ratio of the cell parameters, $c/(2a)$, can be used as a measure of the departure from cubic symmetry.

A. Gibbs–Duhem simulations

The Gibbs–Duhem integration technique, first proposed by Kofke[31,32] has been used to obtain the complete coexistence curve between two phases. The Clapeyron equation,

$$\left(\frac{dp}{dT}\right)=\frac{\Delta h}{T\Delta v}, \tag{2}$$

can be written as

$$\left(\frac{d\ln p}{d\beta^*}\right)=-\frac{\Delta h}{3^*P\Delta v}, \tag{3}$$

where Δh and Δv are the enthalpy and volume changes per particle between both phases. In order to solve Eq. (3), a fourth order Runge–Kutta procedure[35] has been implemented. A different number of cycles were used in the initial and final steps of the Runge–Kutta from the intermediate steps. Long runs were used (between 125 000 and 200 000 cycles) for the initial and final steps in order to determine coexistence densities and enthalpies accurately for each new temperature considered. However, somewhat shorter runs (35 000 cycles) were used for the intermediate steps of the Runge–Kutta procedure since they were used only to estimate the coexistence pressure for the new temperature considered. One cycle consists of a trial move per molecule plus an attempt to change the volume of the system. Given that the points in the Runge–Kutta integration are close one to another, the equilibration phase only includes between 5000 and 10 000 cycles from the configuration of the previous integration step.

For CsCl, 250 ions are used while the sample size is 256 for all the other phases (fluid, CsCl, disordered fcc solid, and tetragonal solid). When implementing the Gibbs–Duhem integration, we used anisotropic NpT for the tetragonal solid and isotropic NpT for each of the other phases.[36] Only translational moves are attempted for the CsCl and tetragonal structures in the Gibbs–Duhem simulations. For the fluid and fcc disordered solids, in addition to translational moves, exchange moves were also included. In an exchange move, a cation and an anion of the system swap their respective positions. The fraction of translational moves is typically 0.8 and the remaining 0.2 are exchange moves. The Gibbs–Duhem simulations were performed on a dual processor computer having AMD Athlon XP 1800+ processors and using OpenMP parallel directives. A Gibbs–Duhem integration with 15 different temperatures typically consumes around one week of CPU. The integration of the Clapeyron equation requires an initial coexistence point. For the fluid-fcc disordered and fluid-CsCl we used the coexistence points from Ref. 22. Namely, for the fluid-fcc disordered solid we used $T^*=0.5$, $p^*=5.64$ as the initial coexistence point. For the fluid-CsCl we used $T^*=0.20$, $p^*=1.91$ as the initial coexistence point. In order to trace the CsCl-tetragonal coexistence line an initial coexistence point is needed. For that purpose free energy calculations were undertaken for both solid structures at $T^*=0.10$ (see details in the next subsection). After performing NpT simulations for both solid struc-

TABLE I. Free energy calculations of the RPM model. For the CsCl structure the maximum value of the translational spring was $\lambda=1000(kT)/\sigma^2$. For the tetragonal structure the maximum value of the translational spring was $\lambda=2500(kT)/\sigma^2$. Ten values of λ were used in the Einstein crystal calculations. Values labeled as Smit *et al.* were taken from Ref. 21.

Phase	T^*	ρ^*	$A/(NkT)$	Source
CsCl	0.05	1.00	−11.06(2)	This work
CsCl	0.05	1.00	−11.05(2)	Smit *et al.*
CsCl	0.10	1.00	−3.13(2)	This work
CsCl	0.10	1.00	−3.09(1)	Smit *et al.*
Tetragonal	0.10	1.20 ($c/(2a)=1$)	−0.73(2)	This work
Tetragonal	0.10	1.20 ($c/(2a)=1.01$)	−0.75(2)	This work
Tetragonal	0.10	1.20 ($c/(2a)=1.02$)	−0.74(2)	This work

tures it was possible to locate the CsCl-tetragonal coexistence point for $T^*=0.10$ at $p^*=1.66$. This was used as the initial coexistence point of our Gibbs–Duhem integration. In summary three initial states were taken for the fluid-fcc disordered solid, fluid-CsCl, and CsCl-tetragonal coexistence curves and Gibbs–Duhem simulations were performed to complete the phase diagram of the model.

B. Einstein crystal calculations

For the calculation of the free energies of the solid phases the Einstein-crystal methodology[28–30] is used. The implementation used here is similar to that described in previous works[37–39] in which the reader should refer to for further details. Translational springs (forcing the atoms to vibrate around the equilibrium lattice position) are used, with a maximum value of $\lambda_{\max}=1000$ (in units of kT/σ^2) for the CsCl structure and $\lambda_{\max}=2500$ for the tetragonal structure. Ten different values of λ have been selected from $\lambda=0$ to $\lambda=\lambda_{\max}$ to perform a Gauss–Legendre integration as described in Ref. 28. For the free energy calculations, 30 000 cycles are generated in the equilibration phase followed by a further 30 000 cycles to obtain thermodynamic averages.

Since the CsCl structure has cubic symmetry, a knowledge of its density is sufficient in order to determine the unit cell parameter. However, this is no longer true for the tetragonal structure for which there are two cell parameters, for instance, a and the ratio $c/(2a)$. For a given density, there remains one independent parameter. This independent parameter has been chosen to be $c/(2a)$. The free energy changes with $c/(2a)$, but, in free energy calculations the cell must have a fixed geometry (the ratio $c/(2a)$ of the equilibrium unit cell should be used). The equilibrium unit cell may be obtained by performing anisotropic NpT simulations and determining the average value of $c/(2a)$ at the desired density. It turns out that the anisotropic NpT simulations yield, for $T^*=0.10$ and $\rho^*=1.20$, an equilibrium value of $c/(2a)$ between 1.01 and 1.02.

In Table I the results of the free energy calculations for the CsCl and the tetragonal systems are presented. In addition, the results from Smit *et al.*[21] for the CsCl structure are included. Our free energy calculations for the CsCl structure agree, to within statistical uncertainties, with those of Smit *et al.*[21] For the tetragonal structure free energy calculations were performed for $c/(2a)=1.00$, 1.01, and 1.02. These three values of $c/(2a)$ were used in order to analyze the effect on the free energy of a small distortion of the ''ideal'' [i.e., $c/(2a)=1$] unit cell. As can be seen in Table I, the Einstein crystal calculations are fully consistent with the results from the NpT simulations since the Helmholtz free energy of the system presents a minimum at constant density for a ratio of $c/(2a)$ between 1.01 and 1.02. Thus, both the free energy calculations and the NpT anisotropic simulations show that, for the selected state, the equilibrium cell of the tetragonal structure has a ratio $c/(2a)$ slightly different from one. Results of Table I allow one to determine the free energy of the ordered solid phases considered in this work. In order to determine the complete phase diagram, the free energies of the fcc disordered solid phase are also required. In Ref. 23 thermodynamic integration was used (along isochores) to obtain the free energy of the disordered fcc solid,

$$\frac{A}{NkT}(\rho^*,\beta^*)=\frac{A}{NkT}(\rho^*,\beta^*=0)+\int_0^{\beta^*}\frac{U}{NkT}\frac{d\beta^*}{\beta^*}. \tag{4}$$

For $T=\infty$ ($\beta^*=0$) the RPM model becomes identical to the hard sphere system except for the presence of an entropy of mixing, $Nk\ln(2)$. The free energy of the solid hard sphere system at any point can be obtained from the free energy calculations of the hard sphere solid of Frenkel and Ladd and the EOS of the hard sphere solid of Hall.[40] Using this procedure for the RPM we obtain at $T^*=0.5$ and $\rho^*=1.20$, $A/(NkT)=5.28\pm0.03$. The free energy for this thermodynamic state can be obtained via a second thermodynamic route. Starting from the value of the free energy of the tetragonal structure at $T^*=0.10$ and $\rho^*=1.20$ reported in Table I, thermodynamic integration [as given by Eq. (4)] is used to compute the free energy of the fcc disordered solid structure. Using this second procedure we obtain $A/(NkT)=5.24\pm0.03$. This second thermodynamic integration is only approximate since it crosses the weakly first order tetragonal-fcc phase transition. Even so, the estimates of the free energy of the fcc disordered structure using these two methods agree to within statistical error.

III. RESULTS AND DISCUSSION

The CsCl and fcc disordered phases present cubic symmetry. The fluid phase is isotropic. Therefore each of these phases can be described correctly either by isotropic NpT or by NVT simulations. This means that our previous NVT simulations of fluid, CsCl and fcc disordered phases as reported in Ref. 22 are still valid and correct (notice however that a misprint occurred in Table VIII our previous work).[41] However, for the tetragonal solid structure anisotropic NpT simulations were used (although the condition that the axes of the simulation box are orthogonal was imposed). In Table II simulation results for the tetragonal structure at $T^*=0.10$ are presented. These results were used to determine the CsCl-tetragonal transition for $T^*=0.10$.

The results of the Gibbs–Duhem simulations for the different coexistence lines considered in this work (fluid-CsCl, CsCl-tetragonal, fluid-fcc disordered) are presented in Table III. The starting point of the Gibbs–Duhem integration is

TABLE II. Simulation results for the tetragonal structure as obtained from anisotropic NpT simulations. The simulations were performed at $T^*=0.10$ with runs of 200 000 cycles. Presented results correspond to the equilibrium density, and residual internal energy.

p^*	ρ^*	$U/(Nk)$
3.0	1.2573	−0.7901
2.7	1.2453	−0.7874
2.5	1.2287	−0.7847
2.2	1.2111	−0.7812
2.0	1.1967	−0.7791
1.8	1.1777	−0.7741
1.6	1.1605	−0.7709

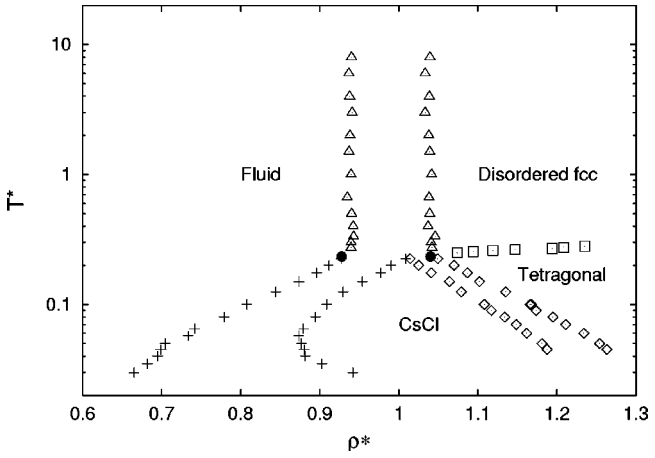

FIG. 2. The phase diagram of the RPM in the $T^*-\rho^*$ plane (log-linear plot). Different symbols are used for each coexistence line; their meaning can be be easily traced from the phases they delimit (not so obvious for the filled circles which represent the fluid-tetragonal solid coexistence data).

labeled with an asterisk. Figure 2 displays the phase diagram in the $T-\rho$ plane. Several interesting features emerge from this plot. The first deals with the fluid-CsCl coexistence line. In our previous work we noticed that, at low temperatures, the density of the CsCl solid at coexistence with the fluid increases as the temperature decreases. The Gibbs–Duhem simulations of this work again confirm this point for temperatures $T^*<0.05$. As a consequence, the RPM exhibits an extremely large volume change upon melting, especially at low temperatures. For $T^*>0.05$, the usual behavior is recovered and the CsCl coexistence density increases with temperature. The second interesting remark is that the fcc disordered-tetragonal transition line at low densities closely approaches the fluid-CsCl-tetragonal triple point. Finally, it is to be stressed that the densities of the fluid-disordered solid coexistence are essentially temperature independent. This has been observed in previous simulations.[22,23] Two theoretical treatments, namely, the cell approximation[22] and the density functional theory[20] have also suggested that this is indeed so. Further on in this paper we shall discuss this point in more detail.

In Fig. 3 the $p-T$ representation of the phase diagram of the RPM model is shown. The extrapolation of the fluid-

TABLE III. Results from Gibbs–Duhem integration obtained in this work. The initial points of the Gibbs–Duhem integration are labeled with an asterisk.

T^*	p^*	ρ_1^*	ρ_2^*	T^*	p^*	ρ_1^*	ρ_2^*
CsCl-Tetragonal				Fluid-CsCl			
0.0450	1.3054	1.1876	1.2631	0.0300	0.0271	0.6650	0.9418
0.0500	1.3310	1.1811	1.2540	0.0350	0.0495	0.6821	0.9027
0.0600	1.3970	1.1617	1.2341	0.0400	0.0737	0.6950	0.8819
0.0700	1.4563	1.1485	1.2111	0.0450	0.0994	0.6989	0.8805
0.0800	1.5370	1.1341	1.1950	0.0500	0.1276	0.7045	0.8767
0.0900	1.6054	1.1170	1.1736	0.0575	0.1749	0.7336	0.8735
0.1000*	1.6600	1.1082	1.1668	0.0650	0.2260	0.7416	0.8795
0.1250	1.8344	1.0791	1.1351	0.0800	0.3458	0.7790	0.8948
0.1500	1.9854	1.0641	1.1020	0.1000	0.5328	0.8076	0.9086
0.1750	2.1198	1.0410	1.0868	0.1250	0.8230	0.8447	0.9298
0.2000	2.2816	1.0251	1.0698	0.1500	1.1545	0.8737	0.9539
0.2250	2.4294	1.0143	1.0493	0.1750	1.5154	0.8962	0.9770
				0.2000*	1.9100	0.9112	0.9903
				0.2250	2.3248	0.9273	1.0088
Fluid-fcc disordered							
0.273	3.036	0.9396	1.0420	Fluid-Tetragonal			
0.300	3.348	0.9397	1.0409	0.2340*	2.4840	0.9277	1.0401
0.333	3.731	0.9428	1.0460	0.2500	2.7088	0.9392	1.0440
0.400	4.494	0.9424	1.0370				
0.500*	5.640	0.9402	1.0391				
0.667	7.552	0.9348	1.0382				
1.000	11.382	0.9397	1.0415				
1.500	17.132	0.9370	1.0391				
2.000	22.882	0.9383	1.0380				
3.000	34.390	0.9410	1.0333				
4.000	45.895	0.9378	1.0387				
6.000	68.909	0.9368	1.0333				
8.000	91.917	0.9401	1.0394				

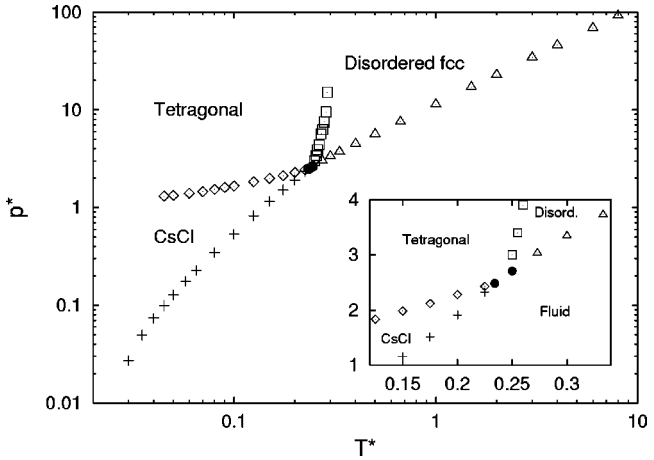

FIG. 3. The phase diagram of the RPM in the p^*-T^* plane. Notice the logarithmic scale of the main plot. The inset is a linear plot of the central region showing the existence of two different triple points each involving the fluid and two solid phases. The meaning of the symbols is the same as in Fig. 2.

CsCl coexistence line to zero pressure provides an estimate of the vapor–liquid–CsCl triple point temperature (the vapor pressures at the vapor–liquid–solid triple point are expected to be very small). From the extrapolation [see Fig. 4(a)] we obtain $T^*=0.0227$. This value agrees very well with that obtained in our previous work. An alternative approach to calculating this triple point is to locate the point where the density of the liquid at coexistence with its vapor becomes identical to that of the fluid in the fluid-CsCl coexistence curve. The vapor–liquid equilibrium of the RPM at the low temperatures considered in this work is unknown. However, a fair estimate of the fluid densities along the vapor–liquid coexistence curve can be obtained by performing zero pressure NpT runs. Results of the zero pressure runs for the liquid phase are presented in Table IV and are depicted in Fig. 4(b). It should be mentioned that the zero pressure densities reported in Table IV are somewhat lower than those reported previously by ourselves in Ref. 22. The origin of the discrepancy is the fact that for such low temperatures very long runs are required in order to obtain fully equilibrated samples and good average values. Results reported in Table IV were obtained by using runs of 400 000 cycles after previously performing 200 000 equilibration cycles. In our previous work[22] we used much shorter runs (10 000 + 10 000 cycles) and it is now clear that those runs were too short to yield good averages for such low temperatures. The new data points reported in Table IV agree with recent calculations of the liquid coexistence density at the triple point temperature performed independently by one of the authors.[12,13] Incidentally, it should be mentioned that the correlation formula proposed by Gillan[42] for the zero pressure densities at low temperatures yields a satisfactory agreement with our new simulation results. Using this procedure, the estimate for the vapor–liquid–CsCl triple point is $T^*=0.0220$ and $\rho^*=0.635$. The uncertainty in the calculation of coexistence densities is higher than for pressures (see, for instance, the noise in the points shown in Figs. 2 and 3). Thus, our final estimate of the vapor–liquid–CsCl triple point temperature should be closer to $T^*=0.0227$ than to $T^*=0.0220$. A reasonable value of $T^*=0.0225$ is in perfect agreement with our previous estimate[22] and close to the value reported by of Smit *et al.*[21]

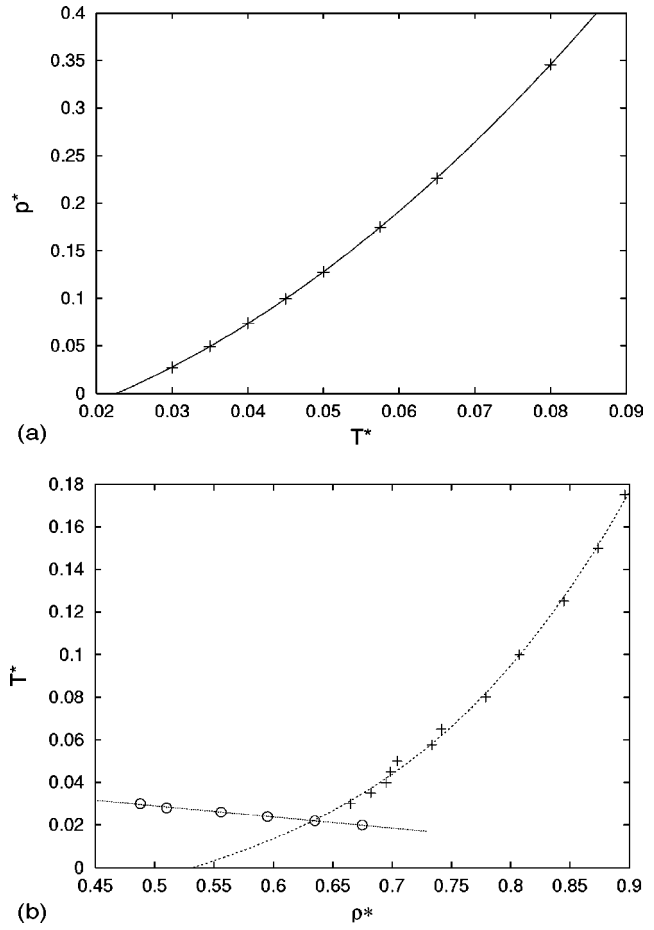

FIG. 4. Extrapolations for the calculation of the vapor–liquid–CsCl triple point. (a) Fit to a second order polynomial of the fluid-CsCl coexistence line in the p^*-T^* plane; (b) fit to a third order polynomial of the fluid-CsCl coexistence line in the $T^*-\rho^*$ plane and its cross with NpT results of the liquid at zero pressure.

TABLE IV. Zero pressure densities of the fluid phase obtained from NpT simulations at zero pressure.

T^*	ρ^*
0.020	0.675
0.022	0.635
0.024	0.595
0.026	0.556
0.028	0.510
0.030	0.488

An interesting feature shown in Fig. 3 is that the slope of the CsCl-tetragonal solid coexistence line is positive and small compared to the other coexistence lines. This can be understood by rewriting the Clapeyron equation as

$$dp/dT=\Delta U/(T\Delta v)+p/T, \tag{5}$$

where ΔU is the change in internal energy at the transition. The second term on the right-hand side is always positive. However, the sign of the first term on the right-hand side depends on the particular transition considered. For most of

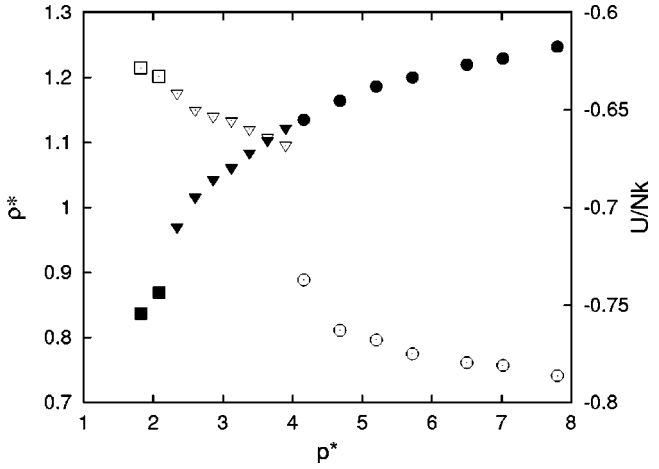

FIG. 5. NpT simulation results for the isotherm $T^*=0.26$. Runs were started with the tetragonal solid at high pressures (circles) which transforms into the disordered fcc phase (triangles) at $p^*=3.9$ and finally melts into the isotropic fluid (squares) at $p^*=2.6$. Open symbols correspond to the internal energy, and filled symbols to the equilibrum density.

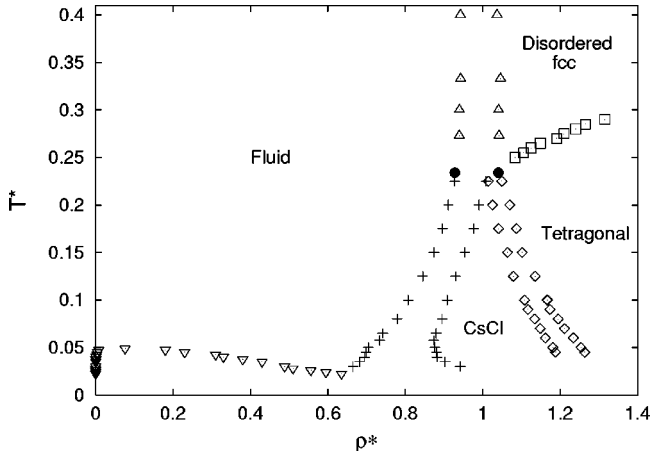

FIG. 6. Global phase diagram of the RPM in the $T^*-\rho^*$ plane. The vapor–liquid equilibrium results were taken from Orkoulas and Panagiotopoulos (see Ref. 7).

the transitions in this work (with the exception of the CsCl-tetragonal solid), it turns out that, when going from the low density to the high density phase (so that Δv is negative), ΔU is also negative (i.e., the high dense phase has a lower internal energy); hence, the first term on the right-hand side is positive, which yields a large slope on the $p-T$ plane. For the CsCl-tetragonal transition Δv is also negative but ΔU is positive, thus the first term on the right-hand side is negative and partially cancels out the positive contribution of the p/T term. This explains the small slope found in Fig. 3 for the CsCl-tetragonal phase transition.

The fluid-disordered solid pressures along the coexistence line fall on an straight line for an enormous range of temperatures (see Fig. 3). In other words, for this transition the slope of the $p-T$ coexistence line is essentially constant. This is certainly striking, but can be explained if one assumes that ΔU is close to zero for the fluid-fcc disordered transition. We shall see that this is indeed a very good approximation. In such a case Eq. (5) can be rewritten as

$$dp/p=dT/T \tag{6}$$

which can be integrated to yield

$$p/T=C, \tag{7}$$

which means that both the slope dp/dT and the ratio p/T in Eq. (5) should be constant. Figure 3 shows that the points corresponding to the fluid-disordered solid coexistence form a straight line. Moreover, the data in Table III allows one to calculate the ratio p^*/T^*. This ratio changes from 11.2 at $T^*=0.30$ to 11.5 at $T^*=8$. At $T^*=\infty$ the freezing of hard spheres is recovered; having $p^*/T^*=11.4$. It is clear that the simulation results are indeed compatible with the assumption that ΔU is close to zero. This provides an indirect evidence of the fulfillment of the assumption, but is it possible to provide more direct evidence? Figure 5 presents NpT simulation results as obtained in this work for $T^*=0.26$. Results for the residual internal energy and for the EOS are also presented. Runs were started from the tetragonal structure at high pressures and then the pressure was slowly decreased. Exchange moves were also included in these simulations. Two phase transitions are clearly visible: the tetragonal-disordered fcc transition—with a very small density jump and a clear energy change that allows to locate the order–disorder transition—and the disordered fcc-fluid transition with a very small energy jump and a clear density change. As can be seen, at the same pressure, the fluid and the fcc disordered solid phases have almost identical internal energies. This means that the approximation $\Delta U=0$ for the fluid-disordered fcc transition is a very good one. A final consequence of the approximation is that the transition entropy, ΔS, should also be constant. This is obtained by writing $\Delta S=(\Delta U+p\Delta v)/T\approx p\Delta v/T$. Since Δv and p/T are almost constant and change little with temperature along the coexistence fluid-disordered fcc line the same must also be true for ΔS.

All coexistence lines seem to cross at a temperature close to $T^*=0.25$. The inset in Fig. 3 shows this region in more detail. Extrapolations of the corresponding coexistence lines indicate that the fluid-CsCl-tetragonal triple point occurs at $T^*=0.234$, $p^*=2.48$. This point is very close to the fluid, fcc disordered and tetragonal solid phases triple point at $T^*=0.245$, $p^*=2.74$. The existence of these two triple points means that direct coexistence between the tetragonal and the fluid phase takes place for a very narrow temperature range (between 0.234 and 0.245). We have confirmed this by computing the fluid-tetragonal equilibrium for $T^*=0.24$. We have found that the tetragonal structure melts into an isotropic fluid before the tetragonal-disordered fcc transition occurs, providing further evidence of the direct coexistence between the tetragonal structure and the fluid. Nevertheless, the tetragonal-fcc disordered transition may show some system size dependence. This fact and the intrinsic statistical error of the simulation may somewhat compromise the existence of this equilibrium, given the narrow range of temperatures where both phases coexist.

In summary three triple points are found for the RPM, a vapor–liquid–CsCl solid triple point, a fluid-CsCl-tetragonal triple point and, finally, a fluid-fcc disordered-tetragonal

triple point. The global phase diagram of the RPM with all phases (including the vapor–liquid equilibria) is presented in Fig. 6. It is interesting to compare the value of the triple point temperature $T_t^*=0.0225$ with that of the critical temperature for this model. For the latter, we adopt here the value $T_c^*=0.0489$ reported by Panagiotopoulos[43] and Caillol *et al.*[44] as the more confident estimate. The ratio of these two values is $T_t^*/T_c^*=0.46$. Purely ionic systems such as NaCl or CsCl present a rather lower value, having $T_t^*/T_c^*\approx 1/3$.[45] The difference between the RPM result and the experimental values for real ionic systems may be due to the disparity in the size of both ions in real substances (compared to the RPM for which the two ions present the same radii). Notice also that the order–disorder transition may be severely affected by small differences in the ionic radii. More work on these issues is needed as to clarify the relevance of the model to real ionic crystals.

Finally, let us mention the large change in volume when the CsCl phase melts at the triple point temperature. Our calculations at the triple point indicate that the fractional density change $(\rho^*_{\text{solid}}-\rho^*_{\text{liquid}})/\rho^*_{\text{solid}}$ is as high as 32%.

IV. CONCLUSIONS

In this work the phase diagram of the RPM model was considered. NpT simulations (isotropic and anisotropic), Einstein crystal calculations and Gibbs–Duhem integration were used to determine the coexistence lines. The picture from this work for the freezing of charged hard spheres is as follows. At high temperatures the freezing occurs into a disordered fcc structure, whereas at low temperatures the freezing occurs into the CsCl structure. At low temperatures and high densities a tetragonal solid is found with a fcc like ordered arrangement of ions. In a very narrow range of temperatures the fluid freezes into the tetragonal ordered structure.

Coexistence densities along the fluid-fcc disordered solid equilibrium do not change much with temperature. For the fluid-CsCl solid equilibrium we found an increase in the solid density as the temperature decreases in the neighborhood of the triple point.

In summary three triple points are found for the RPM, a vapor–liquid–CsCl solid triple point $T^*=0.0225$, a fluid-CsCl-tetragonal triple point $T^*=0.234$, and finally a fluid-fcc disordered-tetragonal triple point $T^*=0.245$.

This works presents a detailed view of the phase diagram of what is probably the simplest model that one can conceive for an ionic system. Since the problem of the fluid–solid equilibrium of ionic system is receiving more and more attention[46–48] a knowledge of the phase diagram may be of interest to workers in the area. This paper shows that a number of interesting features are already present in such a simple model.

ACKNOWLEDGMENT

This work was supported by Project Nos. BFM2001-1420-C02-01 and BFM2001-1017-C03-02 of the Dirección General de Enseanza Superior of Spain.

[1] J. A. Barker and D. Henderson, Annu. Rev. Phys. Chem. **23**, 439 (1972).
[2] J. D. Weeks, D. Chandler, and H. C. Andersen, J. Chem. Phys. **54**, 5237 (1971).
[3] B. P. Chasovskikh and P. N. Vorontsov-Vel'yaminov, High Temp. **13**, 1071 (1975).
[4] P. N. Vorontsov-Vel'yaminov and B. P. Chasovskikh, High Temp. **14**, 174 (1976).
[5] G. Stell, K. C. Wu, and B. Larsen, Phys. Rev. Lett. **37**, 1369 (1976).
[6] G. Orkoulas and A. Z. Panagiotopoulos, Fluid Phase Equilib. **93**, 223 (1993).
[7] G. Orkoulas and A. Z. Panagiotopoulos, J. Chem. Phys. **101**, 1452 (1994).
[8] J. M. Caillol, J. Chem. Phys. **100**, 2161 (1994).
[9] J. M. Caillol and J. J. Weis, J. Chem. Phys. **102**, 7610 (1995).
[10] J. C. Shelley and G. N. Patey, J. Chem. Phys. **103**, 8299 (1995).
[11] F. Bresme, E. Lomba, J. J. Weis, and J. L. F. Abascal, Phys. Rev. E **51**, 289 (1995).
[12] F. Bresme and J. Alejandre, J. Chem. Phys. **118**, 4134 (2003).
[13] M. González-Melchor, J. Alejandre, and F. Bresme, Phys. Rev. Lett. (in press).
[14] D. A. McQuarrie, J. Phys. Chem. **66**, 1508 (1962).
[15] K. S. Pitzer, Chem. Phys. Lett. **105**, 484 (1984).
[16] M. E. Fisher, J. Stat. Phys. **75**, 1 (1994).
[17] M. E. Fisher, in *New Approaches to Problems in Liquid State Theory*, edited by C. Caccamo, J. P. Hansen, and G. Stell (Kluwer, Dordrecht, 1999), pp. 3–8.
[18] G. Stell, in *New Approaches to Problems in Liquid State Theory*, edited by C. Caccamo, J. P. Hansen, and G. Stell (Kluwer, Dordrecht, 1999), pp. 71–89.
[19] F. H. Stillinger and R. Lovett, J. Chem. Phys. **54**, 1086 (1968).
[20] J. L. Barrat, J. Phys. C **20**, 1031 (1987).
[21] B. Smit, K. Esselink, and D. Frenkel, Mol. Phys. **87**, 159 (1996).
[22] C. Vega, F. Bresme, and J. L. F. Abascal, Phys. Rev. E **54**, 2746 (1996).
[23] F. Bresme, C. Vega, and J. L. F. Abascal, Phys. Rev. Lett. **85**, 3217 (2000).
[24] V. Kobelev, A. B. Kolomeisky, and M. E. Fisher, J. Chem. Phys. **116**, 7589 (2002).
[25] N. G. Almarza and E. Enciso, Phys. Rev. E **64**, 042501 (2001).
[26] M. Parrinello and A. Rahman, Phys. Rev. Lett. **45**, 1196 (1980).
[27] S. Yashonath and C. N. R. Rao, Mol. Phys. **54**, 245 (1985).
[28] D. Frenkel and A. J. C. Ladd, J. Chem. Phys. **81**, 3188 (1984).
[29] D. Frenkel and B. Smit, *Understanding Molecular Simulations: From Algorithms to Applications* (Academic, New York, 1996).
[30] P. A. Monson and D. A. Kofke, Adv. Chem. Phys. **115**, 113 (2000).
[31] D. A. Kofke, Mol. Phys. **78**, 1331 (1993).
[32] D. A. Kofke, J. Chem. Phys. **98**, 4149 (1993).
[33] P. P. Ewald, Ann. Phys. (Paris) **64**, 253 (1921).
[34] M. P. Allen and D. J. Tildesley, *Computer Simulation of Liquids*, 2nd ed. (Clarendon, Oxford, 1987).
[35] W. H. Press, B. P. Flannery, S. A. Teukolsky, and W. T. Vetterling, *Numerical Recipes* (Cambridge University Press, Cambridge, 1989).
[36] M. Lisal, R. Budinsky, and V. Vacek, Fluid Phase Equilib. **135**, 193 (1997).
[37] C. Vega, E. P. A. Paras, and P. A. Monson, J. Chem. Phys. **96**, 9060 (1992).
[38] C. Vega and P. A. Monson, J. Chem. Phys. **102**, 1361 (1995).
[39] E. de Miguel and C. Vega, J. Chem. Phys. **117**, 6313 (2002).
[40] K. R. Hall, J. Chem. Phys. **57**, 2252 (1972).
[41] A misprint was found in Table VIII of Ref. 22. The value of Z in the last column of the first 16 rows was written incorrectly. The correct value of Z can be easily obtained by using Eq. (3.3) of that paper and the values of $U/(NkT)$ and $g_{++}(\sigma)$, $g_{-+}(\sigma)$ of Table VIII which are not affected by the misprint.
[42] M. J. Gillan, Mol. Phys. **49**, 421 (1983).
[43] A. Z. Panagiotopoulos, J. Chem. Phys. **116**, 3007 (2002).
[44] J. M. Caillol, D. Levesque, and J. J. Weis, J. Chem. Phys. **116**, 10794 (2002).
[45] A. R. Ubbelohde, *The Molten State of Matter* (Wiley, Chichester, 1978).
[46] B. Guillot and Y. J. Guissani, J. Chem. Phys. **116**, 2047 (2002).
[47] M. Ferrario, G. Ciccoti, E. Spohr, T. Cartailler, and P. Turq, J. Chem. Phys. **117**, 4947 (2002).
[48] J. Anwar, D. Frenkel, and M. G. Noro, J. Chem. Phys. **118**, 728 (2003).